A wind tunnel investigation of the flow across a forest edge

M. Zaschke, B. Ruck

Institute for Hydromechanics, Laboratory of Building- and Environmental Aerodynamics
University of Karlsruhe, Kaiserstrasse 12, 76128 Karlsruhe, Germany

ABSTRACT: The flow across a transition from open land to forest was modeled in an atmospheric boundary layer wind tunnel. Single- and two-point measurements were made using both, laser Doppler and hot wire velocimetry. Due to its large vertical extension a forest edge implies not only a step change in surface roughness but also acts as a spatial obstacle to the approaching flow. Because the depth of the atmospheric boundary layer is much greater than the forest height, the flow behind the edge is strongly influenced by the conditions in the upstream boundary layer.

KEYWORDS: Permeability, surface-mounted obstacle, conditional sampling, windthrow

1 INTRODUCTION

One of the main motivations for investigating the flow across forest edges are concerns about their vulnerability to storm damages. Remarkably, the most exposed trees at the edges themselves are rarely damaged [1], whilst the area affected by windthrow starts at some tree heights behind the edge. The crucial question is, whether critical loads on trees reach their maximal values far from the edges in the interior of the forest under nearly horizontally homogeneous flow conditions or whether there is a zone in the near wake of the edge in which extreme loads exist due to possible transition effects. In the first case, the shape of the forest edge would not be relevant for the risk of storm damages, except for possible damage at the edge trees themselves. In the latter case, it could be beneficial to design forest edges in order to diminish extreme loads further downstream. Even if these loads are possibly restricted to a small critical zone behind the edge, they could create initial gaps in the canopy which make it easy for windthrow to spread downstream and to leave an extensive area damaged. Possible forms of improved forest edge designs are presented and discussed in *Gardiner & Stacey* [2].

The behavior of the flow across forest edges has previously been studied by a number of authors doing field experiments [3], numerical flow simulations [4], or wind tunnel tests. For the wind-tunnel investigation of *Morse et al.* [5], the forest had been composed of nearly ten thousand model trees, constructed in order to account for geometrical and dynamical similarity with real trees.

Aim of the present work was not to reproduce the flow across a forest edge in all its details but rather to investigate some basic aspects of it. Assuming a uniform porosity and perfectly plane vegetation boundaries, a forest edge may be regarded as a forward facing porous step, submerged in a turbulent boundary layer and can easily be modeled using a permeable material. The main advantages of this setup are the clearly defined conditions which can be captured by a few flow parameters and which are believed to allow a simpler interpretation of the measured data.

2 EXPERIMENTAL SETUP

2.1 *Wind tunnel configuration*

The experiments were conducted in a closed-loop atmospheric boundary layer wind tunnel. Similarity with the flow structure in the atmospheric boundary layer is achieved by endowing the bottom surface of the wind tunnel with roughness elements. Vortex generators at the entrance to the test section enforce the rapid formation of a horizontal equilibrium within a short fetch of approximately 3 meters. The scale ratio of the model is 1:200 and, thus, the roughness length of z_0 = 1.55 mm and the boundary layer thickness of δ = 0.6 m correspond to nature values of z_0 = 0.31 m and δ =120 m, respectively.

2.2 *Forest Model*

The vegetation was modeled using a layer of an open-pored permeable polyurethane foam. The thickness of the layer was h = 0.12 m which corresponds to a 24 m high real forest. The pressure loss of a parallel air flow forced to move through the foam had been measured previously and was found to have a magnitude of k_P = 302 m^{-1} ($k_{P,Nature}$ = 1.501 m^{-1}), independently of the Reynolds number. Unfortunately, it is difficult to evaluate whether this value would meet natural conditions. However, from comparisons with the mean velocity field measured in situ around forest edges [5] it may be assumed that the foam represents a rather dense forest.

Belcher et al. [6] introduced a canopy-drag length scale L_C, which is equivalent to the reciprocal of the pressure loss value. The Navier-Stokes equation including the additional body force is thus:

$$\frac{\partial u_i}{\partial t} + u_j \frac{\partial u_i}{\partial x_j} = -\frac{1}{\rho}\frac{\partial p}{\partial x_i} + \nu \frac{\partial^2 u_i}{\partial x_j \partial x_j} + \frac{\left(u_j u_j\right)^{1/2} u_i}{L_C} \tag{1}$$

Assuming Reynolds number independence for wind tunnel conditions and using the model height (h) as a length scale, there are three dimensionless numbers controlling the flow around the forest edge:

- the normalized canopy-drag length scale (L_C/h)
- the ratio of upstream roughness length to model height (z_0/h)
- the ratio of boundary layer thickness to model height (δ/h)

In the present work no variations of the three parameters were made yet and the presented results are based on L_C/h = (1/302)/0.12 = 0.028, z_0/h = 0.00155/0.12 = 0.013 and δ/h = 0.60/0.12 = 5.0, respectively.

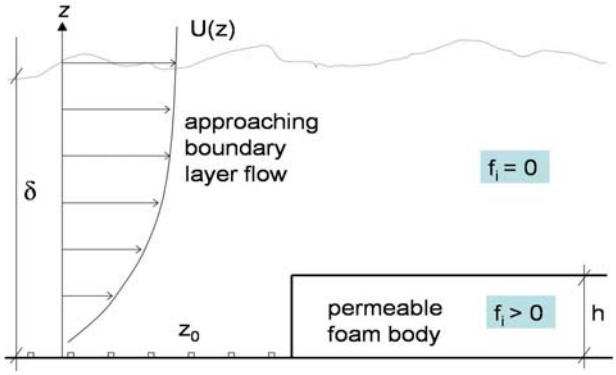

Figure 1. Experimental setup (f_i: additional body force in momentum equation, see eq. 1).

2.3 *Measurement equipment*

Single-point measurements were made using a two-component LDV system operating in a forward scattering light mode. Readings were taken at the measurement points over a period of 52 seconds at a sampling frequency of 500 Hz. In the vicinity of the model edge, where high shear rates and turbulence intensities were to be found, the measuring grid was refined to distances of 5 mm in the vertical and 40 mm in the horizontal. Further measurements were taken with hot wires. Both, a single wire probe and a coplanar triple wire probe were used. The advantage of the triple wire probe is its wider acceptance angle of almost 90° for the incoming flow and its ability to account for lateral fluctuations. A detailed description can be found in *Legg et al.* [7].

Measurements were done at a reference velocity u_{REF} = 10.2 m/s, taken at a height of z = 0.4 m in the free boundary layer flow.

3 RESULTS AND DISCUSSION

3.1 *Single-point statistics*

3.1.1 *Mean velocities and second-order moments*

As shown in Figure 2, in contrast to the case of an impermeable step no recirculation occurs behind the edge. The air partly penetrates the model and is decelerated and directed upwards where it encounters the accelerated free stream flow so that a zone of strong vertical shear is formed.

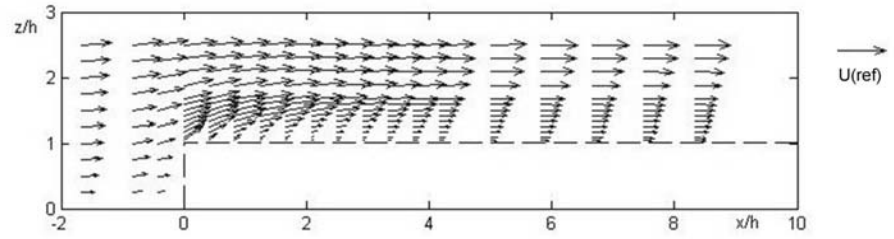

Figure 2. Vector plot of mean velocities.

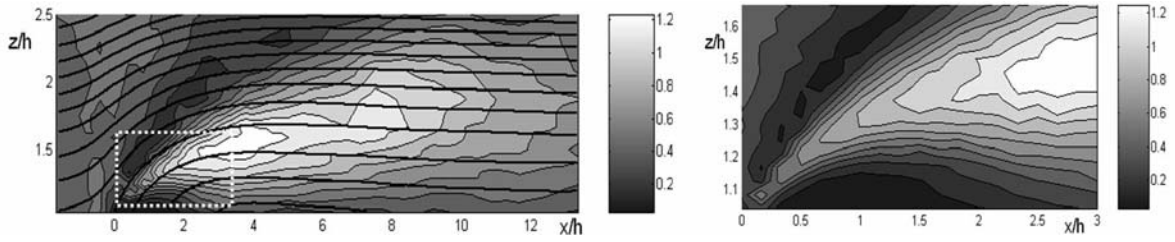

Figure 3. To the left: Reynolds stresses $\overline{u'w'} / u_{REF}^2$ above the model (u': fluctuations in streamline direction, w': fluctuations perpendicular to streamline direction). Thick black lines: streamlines. White dotted frame inside the image: detail (plotted to the right)

Over a distance of about 3 h this shear layer develops freely and grows almost linearly before it gets constrained by the model surface. In the area of attachment maximal values for Reynolds stresses and turbulent kinetic energy can be found (Fig. 3). Further downstream the wake of the

forest edge becomes self-preserving. The dynamics of the shear layer immediately behind the edge is strongly influenced by the turbulence in the upstream boundary layer. Reynolds stresses are transported from the boundary layer into the zone of high vertical mean shear behind the edge where they immediately cause high production rates of the streamwise velocity variance because the dominant production term in the transport equation of $\overline{u'^2}$ is $2\,\overline{u'w'}\cdot\partial\overline{u}/\partial z$.

Morse et al. [5] suggested that production of turbulent kinetic energy occurs primarily in the streamwise component and that further downstream energy is fed into the vertical variance by the return-to-isotropy mechanism. As depicted in Figure 4, turbulence is highly anisotropic close to the edge and then relaxes to a more isotropic state. When the mixing layer attaches to the foam surface, a ratio of about $\overline{u'^2}/\overline{w'^2}$ =1.85 is approached.

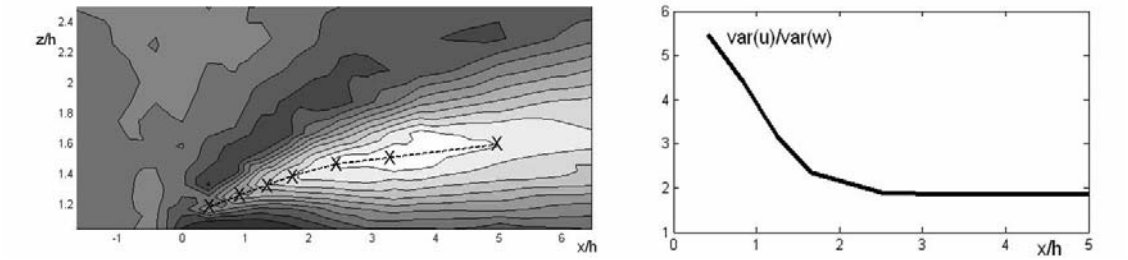

Figure 4. To the left: contour plot of Reynolds stresses with selected points along the central axis of the mixing layer, where the ratio $\overline{u'^2}/\overline{w'^2}$ was evaluated (displayed on right image)

3.1.2 *Third-order moments*

In Figure 5, the skewnesses, i.e. the standardized forms of the third moments of the velocity fluctuations in streamline and cross-stream direction are depicted for the near-edge region. The highly skewed velocity distributions on the low speed side of the mixing layer suggest a comparatively rare but intense intrusion of fast moving air which probably results from a flapping process.

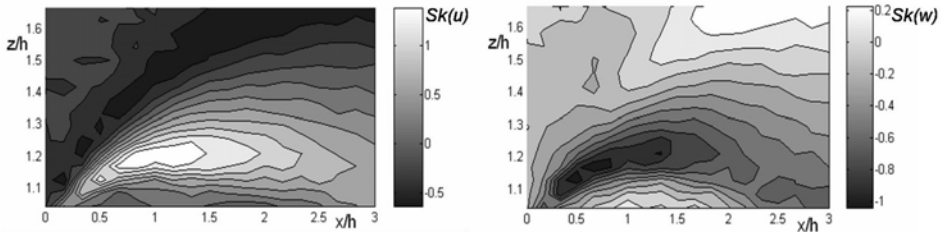

Figure 5. Skewnesses of the velocity distribution in streamline (left) and cross-stream direction (right) for the detail area marked in Fig. 3.

The flapping is caused by the incoming large-scale turbulence which drives a thin local mixing layer up and down and thus enhances the growth of the bulk mixing layer. This mechanism was suggested by *Judd et al.* [8] for the case of shelterbelts. The flapping can be clearly identified only as long as there is a gap between the scales of the growing local eddies in the thin mixing layer and the oncoming large eddies. A view on the energy spectra of the cross-stream fluctuations gives some more insight into the flapping process.

3.1.3 *Energy spectra*

Figure 6 (left image) shows two dominating frequencies: The higher frequency is probably caused by small local eddies resulting from the dynamics of the thin mixing layer. With increasing distance from the edge these eddies grow in size and energy content. A much lower frequency (approximately 4 Hz in the wind tunnel) can be distinguished which is constant and equals the peak frequency of w' in the undisturbed boundary layer. It corresponds to the flapping but can be distinguished clearly only in the early stadium of development of the mixing layer (x < 2 h).

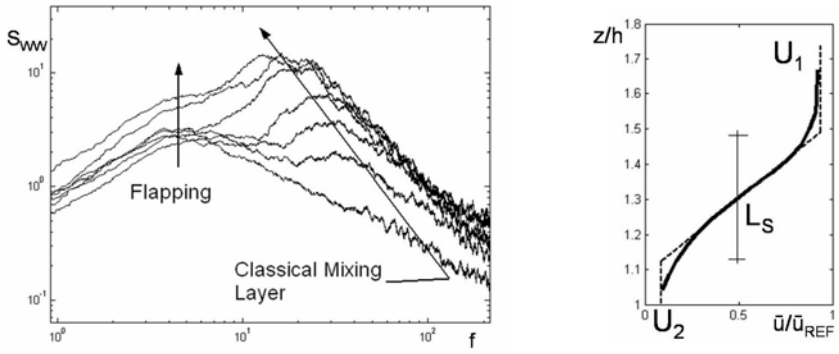

Figure 6. To the left: Energy spectra S_{WW} of fluctuations w' at measurement points indicated in Fig. 5 (arrows indicate increasing distance x from mixing layer origin). To the right: vertical profile of mean velocity at x = 1h with definition of mixing layer width L_S

3.1.4 *Growth of the mixing layer*

The growth of the mixing layer was found to be approximately $dL_S/dx = 0.26$ with the width L_S defined according to Figure 6 (right image). In *Judd et al.* [8] the following relation was suggested to predict the growth rate of the mixing layer behind shelterbelts:

$$dL_S / dx \approx \left[\left(dL_S / dx \right)_{class}^2 + \left(2\sigma_w / \overline{u} \right)_{ambient}^2 \right]^{1/2} \tag{1}$$

where $(dL_S/dx)_{class}$ is the growth rate of a classical mixing layer and $2\sigma_W/\bar{u}$ is the growth rate due to the impact of the upstream vertical fluctuations. The values for the vertical standard deviation σ_W and the horizontal mean velocity $\bar{u}$ have to be taken at z = h in the free flow. Assuming that the first term is comparatively small because of the strongly stable curvature of the mixing layer it is suggested that the relation

$$dL_S / dx \approx \left(2\sigma_w / \overline{u} \right)_{ambient} \tag{2}$$

suffices as a rough approximation. At z = h and at a distance of 2.5 h in front of the edge it was found that $(2\,\sigma_W/\bar{u})_{ambient} = 0.28$, so equation (1) may apply as a crude approximation.

3.1.5 *Inspection of eddy viscosity*

According to mixing length theory, the eddy viscosity may be calculated thus:

$$\nu_t = \beta \cdot u_0 \cdot L_0 \tag{3}$$

where L_0 is a length and u_0 is a velocity scale. For the case of a plane mixing layer L_0 may be identified with the mixing layer width L_S and u_0 may be taken as the difference of the mean velocities on both sides of the mixing layer: $u_0 = U_1-U_2$ (see Fig. 6, right image). Observations of plane, undisturbed mixing layers with $U_2 = 0$ were made by *Schlichting* [9] and *Townsend* [10] and delivered a value of $\beta = 0.014$ for the empirical constant. The eddy viscosity computed with this value compares well with the measured eddy viscosity.

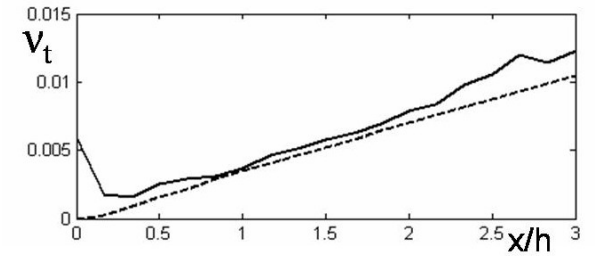

Figure 7. Solid line: measured value for ν_t along middle axis of mixing layer. Dashed line: value for ν_t calculated with $\beta = 0.014$

3.2 *Two-point measurements: Conditional Sampling*

Given single-point statistics only, it is difficult to obtain information about the spatial structure of turbulence. For this purpose, two-point measurements were carried out using hot wire probes. The aim of these measurements was to identify instantaneous flow structures which cause the flapping motion using a conditional sampling procedure.

3.2.1 *Choice of detection criterion and position*

A single wire was placed at x = 1.5 h and z = 1.2 h, i.e. in the area with high positive skewness Sk(u) (see Fig. 5), to measure the horizontal instantaneous velocities. A typical time series of u at this position is printed in figure 7. Velocity peaks could easily be identified by performing a continuous wavelet transformation with a *mexican-hat* wavelet. The detection function was set to D(t) = 1 for the 10 % of the highest wavelet coefficients and D(t) = 0 otherwise.

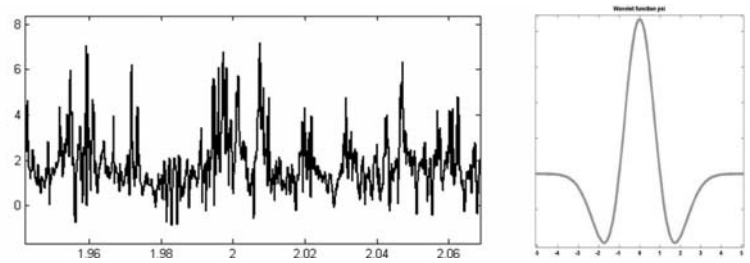

Figure 8: Typical time series of u at detection point (left), Mexican-hat wavelet function (right)

Simultaneously, the instantaneous components of u and w were measured pointwise over the remainder of the flow field between x = -4 h and x = 5 h with the triple wire probe. Given the time series $\mathbf{u}(\mathbf{x},t)$ at point $\mathbf{x}$, the conditional average was computed thus:

$$\hat{\mathbf{u}}(\mathbf{x},\tau) = \overline{\mathbf{u}(\mathbf{x},t+\tau)\cdot D(t)} \,/\, \overline{D(t)} \qquad (4)$$

where τ is an additional phase shift to account for the temporal behavior of the event-triggering motions.

3.2.2 *Results*

The velocity peaks at the detection point are correlated to an eddy-like flow structure approaching from the upstream boundary layer (Fig. 9). The eddy has its center of rotation at the same height as the upper boundary of the forest. It is distorted by the presence of the forest edge and results in a downburst of air further downstream. However, the velocity fields in Figure 9 have to be interpreted with caution because the method used to derive them was based on the rather arbitrary choice of a detection criterion which was chosen to obtain spatial information with little effort. Furthermore, the sampled velocity fields are related only to a certain triggering event at a single point which occurs only in an extreme case and doesn't represent the average flow behavior. The main conclusion which can be drawn from Figure 9 is that eddies of a size of approximately twice the forest height are mainly responsible for the flapping process and for the Reynolds stresses in the shear layer because their rotation induces high instantaneous values of u'w'. Considering the turbulence in the atmospheric boundary layer as a superposition of eddies of different sizes, these critical eddies will always be contained in the eddy spectrum. Unfortunately, no information about the three-dimensional velocity fields and the corresponding pressure fluctuations is available.

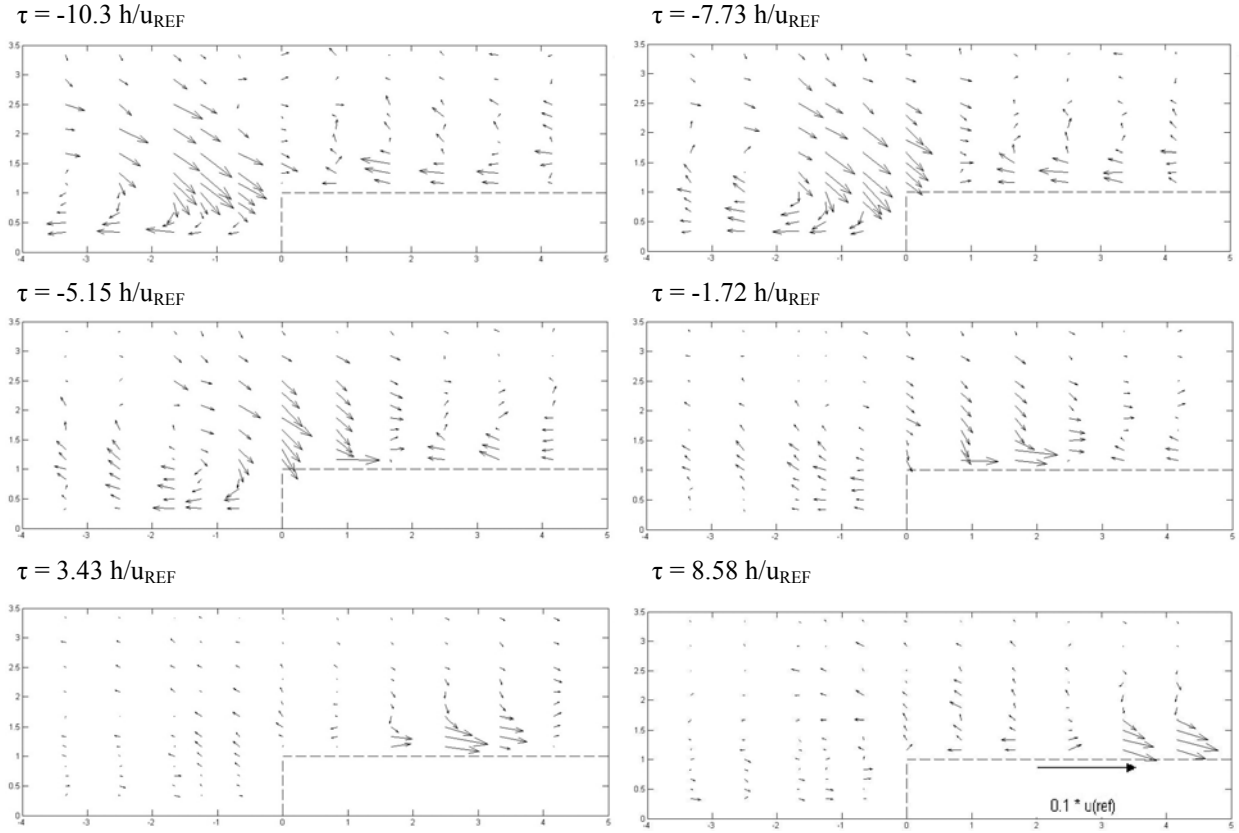

Figure 9. Conditionally averaged velocity field (deviation from mean velocity) for different time shifts before and after detection.

4 CONCLUSION

The flow across the forest edge model is to a large extent determined by the turbulence in the upstream boundary layer. The foam model used in the present study acts as an additional body force on the flow and leads to a distortion of the oncoming boundary layer turbulence. When eddies of the same order of magnitude as the forest edge are exposed to the high mean shear dū/dz above the model, they result in a flapping shear layer and enhance the production of velocity variance in mean streamline direction. This excessive energy is then fed into the vertical variance which in turn drives the production of Reynolds stresses. The free shear layer grows and Reynolds stresses increase with distance from the edge until it attaches to the model surface where maximal stresses and turbulent kinetic energy are reached before the flow becomes self-preserving and slowly approaches horizontal equilibrium. It seems plausible that extreme loads on the trees could be comparatively high in the region of high Reynolds stresses because of the strong gustiness of the flow. However, no direct measurements of forces on the model could be made yet.

The main simplification of the foam model is its uniform porosity which makes it inappropriate for the simulation of a homogeneous canopy flow but which allows to consider the forest edge as a permeable forward facing step.

To gain a more comprehensive view on boundary layer flows across permeable steps it will be necessary to vary the controlling parameters defined in 2.2 and to find similarity solutions for the development of the wake. For the sake of generality it is of interest to cover the whole range of permeabilities from a slight distortion of the boundary layer to the case of a completely impermeable step. Particular attention has to be paid to the dependence of the position and magnitude of the maximal Reynolds stresses on these parameters.

5 REFERENCES

1 K. Fritzsche, Sturmgefahr und Anpassung: Physiologische und technische Fragen des Sturmschutzes, Tharandter Forstliches Jahrbuch, 84 (1933) 1-94.

2 B.A. Gardiner, G. Stacey, Designing Forest Edges to Improve Wind Stability, Forestry commission technical paper 16, Edinburgh, (1996)

3 M.R. Irvine, B.A. Gardiner, M.K. Hill, The evolution of turbulence across a forest edge, Boundary Layer Meteorol., 84 (1997), 467-496

4 B. Yang, R.H. Shaw, K.T. Paw U, Wind loading on trees across a forest edge: A large eddy simulation, Agric. Forest Meteorol., 141 (2006), 133-146.

5 A.P. Morse, B.A. Gardiner, B.J. Marshall, Mechanisms controlling turbulence development across a forest edge, Boundary Layer Meteorol., 103 (2002) 227-251.

6 S.E. Belcher, N. Jerram, J.C.R. Hunt, Adjustment of a turbulent boundary layer to a canopy of roughness elements, J. Fluid Mech., 488 (2003) 369-398.

7 B.J. Legg, P.A. Coppins, M.R. Raupach, A three-hot-wire anemometer for measuring two velocity components in high intensity turbulent boundary layers, J. Phys. E: Sci. Instrum., 17 (1984) 970-976.

8 M.J. Judd, M.R. Raupach, J.J. Finnigan, A wind tunnel study of turbulent flow around single and multiple windbreaks, part I: velocity fields, Boundary Layer Meteorol., 80 (1996) 127-165.

9 H. Schlichting, Boundary Layer theory, McGraw-Hill, New York, 1968, p. 747.

10 A.A. Townsend, The structure of turbulent shear flow, Cambridge University Press, Cambridge, 1976, p. 224